Zhang et al. *Zool. Res.* 2025, 46(5): 1108−1120
https://doi.org/10.24272/j.issn.2095-8137.2025.050
https://cstr.cn/32248.14.zr.2025.050

ZR | Zoological Research

Article Open Access

CircSHOC2 regulates steroid hormone synthesis in ovarian granulosa cells through the mir-130b-5p/ASH1L pathway

Lu-Tong Zhang[1,#], Teng Zhang[1,#], Xiang-Rong Song[1], Madaniyati Mie-Lie[1], Yi-Hao Li[1], Lei Gao[1], Gong-She Yang[1,*], Gui-Yan Chu[1,*]

[1] *College of Animal Science and Technology*, *Northwest A & F University*, *Yangling*, *Shaanxi* 712100, *China*

ABSTRACT

Estrus represents a critical phase in the porcine reproductive cycle and relies on functional ovarian development and coordinated steroidogenesis. Granulosa cells (GCs) mediate these processes by secreting estradiol (E_2) and progesterone (P_4), which are essential for follicular maturation and ovulatory competence. While circular RNAs (circRNAs) have been implicated in steroid hormone synthesis, their involvement in the regulation of gilt estrous remains unclear. In this study, circRNA sequencing was performed on ovarian tissues of estrus (ES) and non-estrus (NES) gilts, resulting in the identification of a novel circRNA, termed circular SHOC2 leucine rich repeat scaffold protein (circSHOC2), which exhibited marked up-regulation in ES ovaries. Functional assays demonstrated that circSHOC2 overexpression enhanced E_2 and P_4 synthesis and increased the protein levels of key steroidogenic enzymes. Mechanistic investigation revealed that circSHOC2 sponges miR-130b-5p. Silencing miR-130b-5p significantly enhanced E_2 and P_4 production, along with the up-regulation of steroidogenic proteins. Additionally, miR-130b-5p targeted ASH1-like histone lysine methyltransferase (ASH1L), while its overexpression significantly inhibited ASH1L. Cotransfection experiments revealed that ASH1L mitigated the inhibitory effects of miR-130b-5p on E_2 and P_4 synthesis in GCs. These findings establish a regulatory axis in which circSHOC2 modulates steroidogenic capacity in porcine GCs via the miR-130b-5p/ASH1L pathway, offering mechanistic insight into the molecular basis of gilt estrus and providing potential targets to enhance reproductive efficiency.

Keywords: Gilt estrus; CircRNA; miR-130b-5p; ASH1L; Steroid hormone

INTRODUCTION

Efficient gilt reproduction underpins herd productivity and directly influences the profitability of commercial swine production. However, approximately 10% of gilts fail to exhibit their first estrus by 8 months of age and are eliminated from breeding programs (Xin et al., 2018). Estrus onset is orchestrated by follicular development within the ovary, during which granulosa cell (GC)-derived estrogen signals the brain to initiate estrous behavior (Dial et al., 1983). Impaired follicular development disrupts steroidogenesis and represents a primary cause of estrous failure in gilts (Knox, 2024; Langendijk et al., 2000). Estradiol (E_2) and progesterone (P_4), the principal steroid hormones synthesized by ovarian GCs (Feng et al., 2019; Kolesarova et al., 2017; Rodway et al., 1999; Sirotkin, 1994), are essential for orchestrating follicular maturation (Ting et al., 2015), regulating estrous cyclicity (Domingues et al., 2023), and supporting early pregnancy (Geisert et al., 2024). Although steroid hormone synthesis is influenced by genetic predisposition (Liu et al., 2024), nutritional status (Xiong et al., 2024), and environmental factors (Knox, 2024), the precise mechanisms underlying regulatory networks remain poorly understood. Enhancing steroidogenic output in GCs therefore offers a promising strategy to promote estrus onset and improve reproductive efficiency in gilts (Am-In et al., 2020; Ziecik et al., 2020).

Circular RNAs (circRNAs), a subclass of noncoding RNAs (ncRNAs), are known for their tissue-specific, cell-specific, and developmental stage-specific expression patterns (Jeck et al., 2013; Ma et al., 2023). Multiple studies have documented circRNA expression changes during ovarian development, folliculogenesis, and the estrous cycle across various species, including mice (Jia et al., 2018), pigs (Liang et al., 2017), cattle (Fu et al., 2018), and goats (Xu et al., 2021). While these findings suggest that circRNAs play an important role in the estrous cycle and follicular development, their expression dynamics and regulatory functions during estrus (ES) and non-estrus (NES) stages in gilts remain uncharacterized. Our

Received: 18 March 2025; Accepted: 15 April 2025; Online: 16 April 2025
Foundation items: This work was supported by the National Key Research and Development Program of China (2022YFD1300303; 2021YFF1000602), National Natural Science Foundation of China (32472878), and China Agriculture Research System (CARS-35-PIG)

[#]Authors contributed equally to this work

*Corresponding authors, E-mail: gsyang@nwafu.edu.cn; guiyanchu@nwafu.edu.cn

research identified a novel circRNA, circular SHOC2 leucine rich repeat scaffold protein (circSHOC2), which regulates GC steroid hormone synthesis via the miR-130b-5p/ASH1-like histone lysine methyltransferase (ASH1L) pathway.

CircRNAs regulate mRNA translation by acting as molecular sponges for microRNA (miRNA) response elements (MREs), thereby preventing miRNAs from binding to their target mRNAs (Patop et al., 2019). Transcriptomic and functional analyses identified miR-130b-5p as a direct target of circSHOC2. Although miR-130b-5p has been implicated in tumorigenesis (Chen et al., 2018; Zhang et al., 2019), cell proliferation (Feng et al., 2024), and lipid metabolism (Liu et al., 2020), its biological significance in reproductive endocrine function remains unclear. This knowledge gap underscores the need to investigate downstream effectors mediating its influence on ovarian steroidogenesis.

Comprehensive analyses have identified ASH1L as a direct target of miR-130b-5p and a critical hub connecting upstream regulatory signals to downstream steroidogenic pathways. ASH1L encodes a histone methyltransferase that catalyzes H3K36-specific modifications (Miyazaki et al., 2013) and contributes to cellular differentiation (Xia et al., 2017), embryonic development (Brinkmeier et al., 2015), and cell proliferation (Li et al., 2017). Aberrant ASH1L expression disrupts ovarian homeostasis: overexpression in mouse oocytes induces apoptosis, depletes primordial follicle pools, and accelerates reproductive senescence (Zhang et al., 2022b), while its suppression in cumulus cells impairs proliferation and promotes apoptosis (Cui et al., 2021). These findings imply that ASH1L is a key modulator of female reproductive physiology. Nevertheless, its potential involvement in steroid hormone biosynthesis has yet to be clarified.

In this study, circRNA sequencing of ovaries from ES and NES gilts revealed circSHOC2 as the most significantly differentially expressed transcript. Functional investigations demonstrated that circSHOC2 enhances steroid hormone synthesis in GCs by sponging miR-130b-5p and relieving post-transcriptional repression of ASH1L. These results identify circSHOC2 as a previously unrecognized regulator of GC steroidogenic function and establish a mechanistic link between noncoding RNA signaling and ovarian endocrine activity.

MATERIALS AND METHODS

Estrus identification in gilts

From 160 days of age, New French Yorkshire gilts were exposed to mature boars twice daily for over 30 min per session to stimulate estrus expression, using boars as the primary stimulus and BOAR BETTER pheromones (Vetoquinol, France) as a supplemental cue (McGlone et al., 2023). Beginning at 165 days, estrus-related behaviors and timing were recorded using individual file cards. Estrus was identified based on external genital changes, including vulvar redness, swelling, mucous discharge, and positive standing reflex (Yang et al., 2018). Vulvar morphology was monitored to classify gilts as non-estrus, in diestrus, or in estrus (Supplementary Figure S1). Postmortem examination of ovarian morphology, follicular development, and corpus luteum presence confirmed the absence of silent estrus or ovarian cysts in NES gilts (Supplementary Figure S2).

Sample selection and preparation for sequencing

Sample selection criteria for ES and NES gilts followed protocols established in previous studies (Shi et al., 2023b). At a breeding pig farm in Shaanxi Province, 643 healthy, lineage-verified New French Yorkshire sows with at least three parities (average litter size ≥12.5) and a minimum of seven pairs of teats were selected as the maternal stock to establish the core breeding population (C0 generation). From 102 litters (290 C1 generation gilts), estrus detection commenced at 165 days of age. Gilts exhibiting two consecutive estrus cycles were classified as ES, those displaying a single estrus cycle were designated as irregular, and those showing no signs of estrus were defined as NES. Of the 102 litters, 24 consisted entirely of ES gilts, 12 consisted entirely of NES gilts, and 32 exhibited irregular estrus patterns. In the remaining 34 litters, both ES and NES gilts were present. To study the differences between full-sibling individuals with estrus and non-estrus, we excluded 4 litters with inconsistent body condition from the 34 litters that met the experimental requirements, ultimately selecting 30 litters. From the same litter, one ES gilt and one NES gilt were selected, and the ES gilt was slaughtered during its third estrus period. A total of 6 groups were slaughtered, including 6 ES gilts and their corresponding full-sibling NES gilts. The right ovaries were frozen and stored at –80°C for subsequent sequencing result verification, while the left ovaries were used for circRNA sequencing. All animal protocols were approved by the Committee for the Ethics on Animal Care and Experiments of Northwest Agriculture and Forestry University (No. NWAFU-202106025).

CircRNA sequencing and identification

Total RNA was extracted from ovarian tissue samples (Supplementary Table S1), and ribosomal RNA was removed to construct a strand-specific library. The library was prepared for sequencing using the Illumina NovaSeq™ 6000 platform (USA), with a paired-end sequencing read length of 2×150 bp. Raw reads were processed to remove adapters and low-quality reads (Supplementary Table S2). Clean reads were aligned to the *Sus scrofa* reference genome Sscrofa11.1 using HISAT (Kim et al., 2015). Analysis was performed based on the gene location information in the genome annotation file (Supplementary Table S3).

CircRNA identification was performed using CIRCexplorer2 and CIRI (Gao et al., 2015; Zhang et al., 2016), which detect circRNAs based on their structural and splicing sequence features. The prediction results from both tools were integrated by overlapping the predicted circRNA start and end sites. Candidate circRNAs were then annotated according to their genomic locations and gene associations. HTSeq was used to quantify circRNA expression as read counts, which were normalized to RPM values. The number of splicing site sequences was also determined (Anders et al., 2015).

Primary culture and transfection of porcine ovarian GCs

Primary porcine GCs were isolated and cultured following previously described protocols (Gao et al., 2023b). Ovaries (n= 30) were collected from healthy pigs at the Yangling Benxiang Group slaughterhouse. Ligaments were removed, and the ovaries were incubated at 37°C in normal saline containing 100 U/mL penicillin/streptomycin. Healthy follicles measuring 3 –5 mm in diameter were selected, and follicular fluid containing GCs was aspirated using a 20 mL syringe. The suspension was subsequently centrifuged at 800 ×g for 10 min at 17°C, after which the supernatant was discarded. The cell pellet was resuspended in Dulbecco's Modified Eagle Medium/Nutrient Mixture F-12 (DMEM/F12) containing 10% fetal bovine serum

(FBS). Cells were dispersed by repeated pipetting, seeded into culture plates at 10^5 cells/cm^2, and incubated at 37°C in a 5% CO_2 atmosphere. After 24 h, non-adherent cells were removed by washing with phosphate-buffered saline (PBS), and fresh medium was added for continued culture. Cells were subcultured once they reached 50%–60%. After 24 h of transfection, both the culture medium and cells were harvested for further analysis. GCs were transfected using the following reagents: circSHOC2-PCD5 (1 000 ng/mL, Guangzhou Jisai Biotech, China), si-circSHOC2, the miR-130b-5p inhibitor, the miR-130b-5p mimics, and si-ASH1L (50 nmol/L, Shanghai Jima Biotech, China). All reagents were used according to the manufacturer's protocols. Sequence information is provided in Supplementary Table S4. Experimental replicates were set according to the requirements of each assay.

RNA isolation and reverse transcription quantitative PCR (RT-qPCR)

Total RNA was extracted from treated GCs, and expression levels of steroid hormone–related mRNAs were measured using RT-qPCR. cDNA was synthesized from 500 ng of total RNA using the HiScript III RT SuperMix for qPCR (Vazyme, China). RT-qPCR was performed with SYBR PCR mix (Vazyme, China) on a StepOne Real-Time PCR system (ABI, USA). Each reaction contained 25 ng of cDNA and 400 nmol/L primers, with *β-actin* used as the internal control. Relative mRNA expression levels were calculated using the $2^{-\Delta\Delta Ct}$ method. Primer specificity and amplification efficiency ranged from 90% to 110%. Each experimental group included at least three biological replicates and three technical replicates. Primer sequences and RT-qPCR thermal cycling conditions are provided in Supplementary Tables S5, S6.

Western blot analysis

Western blotting was performed with three biological replicates per experimental group. Cultured GCs were lysed using ice-cold radio immunoprecipitation assay (RIPA) protein lysis buffer (Beyotime, China) supplemented with a protease inhibitor (Pierce, USA). Equal amounts of protein (20 μg) were separated using 12% sodium dodecyl sulfate-polyacrylamide gel electrophoresis (SDS-PAGE), with a tri-color prestained protein marker (WJ103, Yamei, China) used to indicate molecular weights. The separated proteins were transferred onto polyvinylidene difluoride (PVDF) membranes (Cell Signaling Technology (CST, USA)) and incubated (4°C, 8h) with the following primary antibodies: anti-cytochrome P450 family 11 subfamily A member 1 (CYP11A1) (ab232763, 60 kDa, 1:1 000, rabbit, Abcam, UK), anti-3β-hydroxy steroid dehydrogenase (3β-HSD) (ab167417, 42 kDa, 1:1 000, rabbit, Abcam), anti-cytochrome P450 family 19 subfamily A member 1 (CYP19A1) (ab106168, 58 kDa, 1:1 000, rabbit, Abcam, UK), anti-steroidogenic acute regulatory protein (StAR) (8449S, 28 kDa, 1:1 000, rabbit, CST, USA), and anti-cytochrome P450 family 17 subfamily A member 1 (CYP17A1) (ab125022, 55 kDa, 1:1000, rabbit, Abcam, UK). β-ACTIN (sc-47778, 43 kDa, 1:1 000, mouse, Santa Cruz, USA) was used as a loading control. Subsequently, the membranes were incubated (17°C, 2h) with horseradish peroxidase (HRP)-conjugated secondary antibodies: mouse anti-rabbit immunoglobulin G (IgG) (sc-2357, 1:5 000, Santa Cruz, USA) and goat anti-mouse IgG (sc-2005, 1:5 000, Santa Cruz, USA). Protein signals were detected using the iBright 1500 system (Thermo Fisher Scientific, USA) and quantified with ImageJ software (http://imagej.nih.gov/ij/).

Luciferase reporter assay

Luciferase reporter plasmids (psi-CHECK2) containing wild-type circSHOC2 (circSHOC2-WT), mutant circSHOC2 (circSHOC2-Mut), wild-type 3' untranslated region (3'UTR) of ASH1L (ASH1La-WT), and mutant 3'UTR of ASH1L (ASH1Lb-Mut) were constructed by General Biosystems (China). Sequence information of all WT and mutant constructs is shown in Supplementary Table S7. HEK293T cells were seeded in 48-well plates, and cotransfected with WT or MUT 3′UTR luciferase reporter plasmids, along with miRNA mimics or negative control, using Lipofectamine 2000 (Thermo Fisher Scientific, USA). After 24 h of transfection, the cells were harvested, and luciferase activity was quantified using the Dual-Glo Luciferase Assay System (Promega, USA) according to the manufacturer's instructions. Firefly luciferase activity was used for normalization. Each experimental group included three biological replicates.

Enzyme-linked immunosorbent assay (ELISA)

E_2 levels were measured using a porcine E_2 ELISA kit (YJ002366, Yuanju Biotechnology Center, China) following the manufacturer's instructions. The kit exhibited intra-assay and inter-assay coefficients of variation (CV) below 10% and 15%, respectively, and a sensitivity range of 2.5–200 pg/mL. P_4 levels were measured with a porcine P_4 ELISA kit (YJ002422, Yuanju Biotechnology Center, China), with an intra-assay CV < 10%, inter-assay <15%, and a sensitivity range of 0.625–20 ng/mL. Absorbance was recorded at 450 nm using a Multiskan™ FC spectrophotometer (Thermo Fisher Scientific, USA). Both kits employed monoclonal antibodies with no cross-reactivity. Each experimental group included four biological replicates.

Bioinformatics analysis

Potential miRNAs targeting circSHOC2 were predicted using TargetScan (http://www.targetscan.org) and miRanda (http://mirtoolsgallery.tech/mirtoolsgallery/node/1055). Candidate target genes of miR-130b-5p were identified using TargetScan (http://www.targetscan.org), miRDB (http://mirdb.org/), and miRwalk (http://mirwalk.umm.uni-heidelberg.de/). Predictions were made by inputting the sequences and gene names of circSHOC2 and miR-130b-5p and selecting appropriate species. RNAhybrid (https://bibiserv.cebitec.uni-bielefeld.de/rnahybrid/) was used for sequence binding analysis and free energy prediction of target genes. Gene Ontology (GO) and Kyoto Encyclopedia of Genes and Genomes (KEGG) pathway analyses were performed via KOBAS v.3.0 (http://kobas.cbi.pku.edu.cn/index.php).

RNase R digestion assay

Each experimental group included three biological replicates. Total RNA was extracted from GCs and incubated with the RNase R digestion kit (RNR07250, Epicentre Biotechnologies, USA) at 37℃ for 30 min to selectively degrade linear RNA while preserving circRNA. The resulting RNA was reverse transcribed and amplified by RT-qPCR. Amplification products were assessed by gel electrophoresis to confirm circRNA resistance to RNase R digestion.

Cytoplasmic and nuclear RNA purification

Each experimental group included three biological replicates. Cytoplasmic and nuclear RNA were isolated using the Cytoplasmic and Nuclear RNA Purification Kit (CH-21000, Norgen BioTek, Canada). Briefly, GC suspensions were centrifuged at 1000 ×*g* for 10 min at 4°C, lysed with lysis buffer, and separated into cytoplasmic (supernatant) and nuclear

(pellet) fractions by centrifugation (20 000 ×*g* for 10 min at 4°C). Each fraction was mixed with buffer and ethanol, transferred to a spin column, washed, and eluted. Purified RNA was stored at −80℃ for downstream applications.

Statistical analysis

Experimental data were analyzed using GraphPad Prism v8 (https://www.graphpad-prism.cn/). Results are presented as mean±standard error of the mean (SEM) based on at least three biological replicates. Comparisons between two groups were performed via two-tailed unpaired Student's *t*-tests. Comparisons involving three or more groups were determined using one-way or two-way analysis of variance (ANOVA), followed by Dunnett and Sidak *post hoc* tests, respectively. Statistical significance was denoted as ns: Not significant; *: P<0.05; **: P<0.01; ***: P<0.001; ****: P<0.0001.

RESULTS

Identification and differential profiling of ovarian circRNAs in ES and NES gilts

New French Yorkshire gilts with a shared genetic background and identical feeding conditions were categorized into the ES and NES groups following standardized estrus detection protocols (Figure 1A). Morphological examination of reproductive organs revealed that NES gilts exhibited smaller ovaries and uteri, with no visible mature follicles or corpora lutea (Figure 1B, C). Serum E_2 and P_4 levels were significantly lower in the NES group compared to the ES group (Figure 1D), confirming the absence of silent estrus and validating the selection criteria for transcriptomic analysis.

High-throughput circRNA sequencing of ovarian tissue, followed by systematic bioinformatic analysis, identified 17 662 distinct circRNAs across all samples, including 3 919 present in both the NES and ES groups (Figure 1E, F). Host gene annotation revealed 5 275 protein-coding genes, with 2 846 shared between groups, representing 54.0% of all host genes (Figure 1G, H). Notably, 37.18% of the genes produced a single circRNA, while the remaining genes generated two or more circRNAs (Figure 1I). Chromosomal mapping demonstrated genome-wide circRNA distribution, with pronounced density on chromosome 12. Most circRNAs spanned multiple genomic regions, with only a small fraction originating from a single exon, intron, or intergenic region (Figure 1J).

Further analysis identified 67 differentially expressed circRNAs (DECs) between the ES and NES groups ($-\log_{10}$ (P-value)>1.301, $|\log_2$(fold change)|>1) (Supplementary Table S8), including 30 up-regulated and 37 down-regulated candidates (Figure 2A, B). Chromosomes 1 and 6 harbored the highest number of DECs (Figure 2C). Notably, the *CUL1* gene encoded two significantly up-regulated circRNAs (circRNA1422 and circRNA1794) in ES ovaries, while all other host genes encoded only a single circRNA.

Cross-referencing with public circRNA databases revealed that 55 DECs originated from annotated host genes, while 11 mapped to intergenic regions. GO enrichment analysis indicated functional association of host genes with the Arp2/3 protein complex, mRNA processing body assembly, ubiquitin ligase complex, RNA phosphodiester bond hydrolysis, and regulation of estradiol secretion (Figure 2D). KEGG pathway analysis further highlighted enrichment in pathways related to TGF-β signaling, ECM-receptor interaction, actin regulation, and p53 signaling (Figure 2E). To validate sequencing-based differential expression profiles, six circRNAs were selected for RT-qPCR. All six circRNAs exhibited expression trends consistent with the high-throughput sequencing data. Among them, circ1855 showed the highest fold change and was derived from the *SHOC2* gene. This circRNA was subsequently designated as circSHOC2 (Figure 2F, G).

Overall, circRNA transcriptome profiling of ES and NES gilts yielded a comprehensive ovarian circRNA atlas and identified circSHOC2 as a key differentially expressed transcript potentially linked to estrous regulation.

CircSHOC2 promotes steroid hormone synthesis in GCs

CircSHOC2 was generated via back-splicing of exon 4 of the *SHOC2* gene and spanned 943 base pairs in length (Figure 3A), with RNase R digestion confirming a stable circular structure (Figure 3B, C). RT-qPCR revealed significantly higher expression of circSHOC2 in ES ovaries relative to NES ovaries (Figure 3D). Subcellular fractionation further indicated predominant localization of circSHOC2 in the cytoplasmic compartment of GCs (Figure 3E), suggesting a post-transcriptional regulatory role.

Functional assays in primary porcine GCs revealed that silencing circSHOC2 with si-circSHOC2 significantly suppressed its expression (Figure 3F), leading to a marked reduction in E_2 and P_4 concentrations in the culture supernatant compared with the control group (Figure 3G). Concomitantly, both mRNA and protein levels of key steroidogenic genes, including *CYP11A1*, *CYP19A1*, and *3β-HSD*, were also substantially reduced following circSHOC2 knockdown (Figure 3H−J). In contrast, overexpression of circSHOC2 through the circSHOC2-PCD5 vector (Figure 3K) resulted in elevated steroid hormone levels (Figure 3L), accompanied by significant up-regulation of CYP11A1, CYP19A1, and 3β-HSD at both transcript and protein levels (Figure 3M−O). Collectively, these findings suggest that circSHOC2 plays a role in promoting steroid hormone synthesis in porcine GCs by modulating the expression of key enzymes involved in steroidogenic pathways.

CircSHOC2 modulates steroidogenesis in GCs through direct interaction with miR-130b-5p

To elucidate the regulatory mechanism by which circSHOC2 influences steroid hormone biosynthesis in GCs, miRNAs potentially targeted by circSHOC2 were predicted using TargetScan and miRanda online tools (Figure 4A). Integration of these predictions with miRNA sequencing (miRNA-seq) data from ES and NES ovaries, followed by expression profiling and seed sequence complementarity analysis, highlighted miR-130b-5p as a high-confidence target. Quantitative analysis revealed significantly lower expression of miR-130b-5p in ES ovaries compared to NES ovaries (Figure 4B). Binding site prediction confirmed a complementary interaction between miR-130b-5p and circSHOC2, with a calculated binding free energy of −22.4 kcal/mol (Figure 4C).

Dual-luciferase assays were performed using psiCHECK2 constructs carrying WT or mutated circSHOC2 binding sites (circSHOC2-WT and circSHOC2-Mut, respectively; Figure 4D). Overexpression of miR-130b-5p significantly reduced luciferase activity of circSHOC2-WT but had no effect on circSHOC2-Mut activity, confirming that miR-130b-5p is a direct target of circSHOC2 (Figure 4E). Additionally, co-transfection of circSHOC2-PCD5 with miR-130b-5p mimics significantly increased miR-130b-5p levels compared with the control (circSHOC2-PCD5+mimics NC) (Figure 4F).

Inhibition of miR-130b-5p in primary ovarian GCs led to a

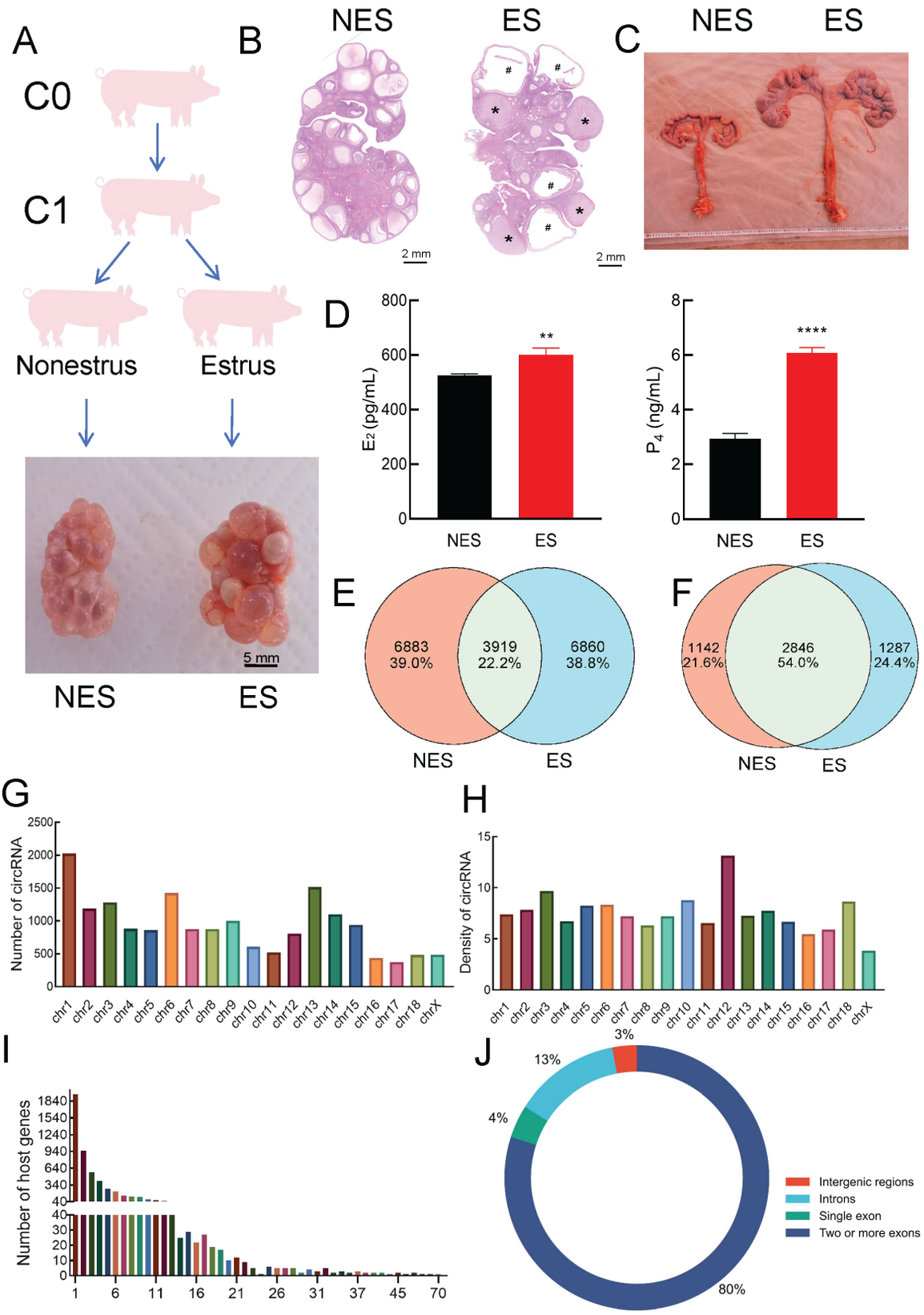

Figure 1 CircRNA expression profiles in ovaries of ES and NES gilts

A: Selection process for ES and NES ovarian samples. B: Representative H&E-stained ovarian sections from NES and ES groups; scale bars, 2 mm. #: Large follicle; *: Corpus luteum. C: Representative uterine morphology in NES and ES groups. D: Serum concentrations of E_2 and P_4. **: $P<0.01$; ****: $P<0.0001$. E: Number of circRNAs identified in ES and NES ovaries. F: Number of host genes associated with circRNAs. G: Number of circRNAs identified on each chromosome. H: Distribution density of circRNAs across chromosomes, expressed as number of circRNAs per megabase (Mb) of chromosome length. I: Number of circRNAs produced by host genes. J: Composition analysis of circRNAs, indicating proportions derived from multiple exons, single exons, single introns, and intergenic regions.

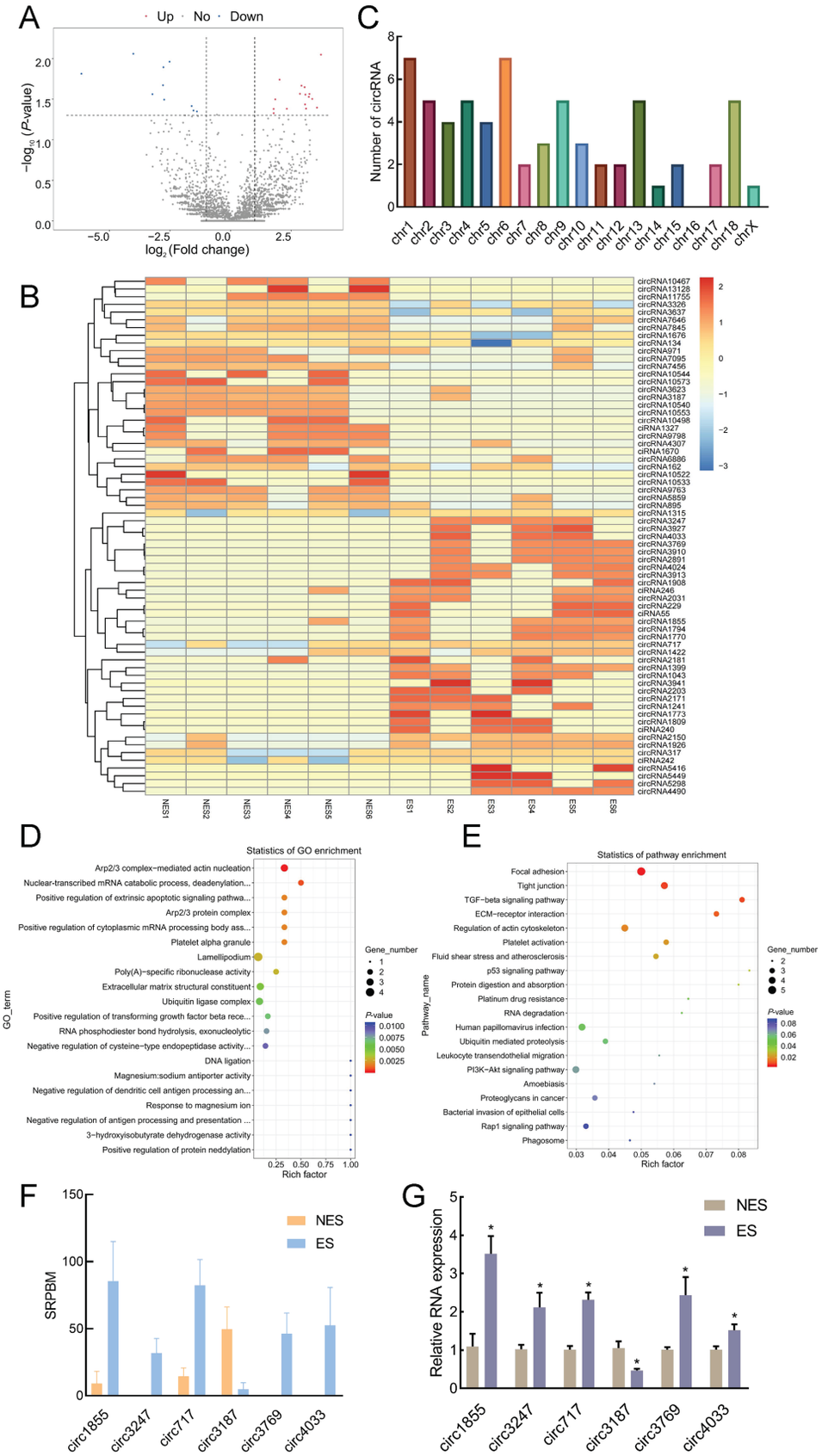

Figure 2 Functional annotation and validation of host genes of differentially expressed circRNAs

A: Volcano plot showing differentially expressed circRNAs. B: Heatmap showing expression profiles of differentially expressed circRNAs. C: Chromosomal locations of differentially expressed circRNAs. D: Bar chart showing GO enrichment analysis results. E: Bubble chart showing top 20 KEGG enriched pathways. F: Expression levels of circRNAs identified through sequencing in ES and NES ovaries. G: Validation of circRNA expression in ES and NES ovaries by RT-qPCR, n=6. *: P<0.05.

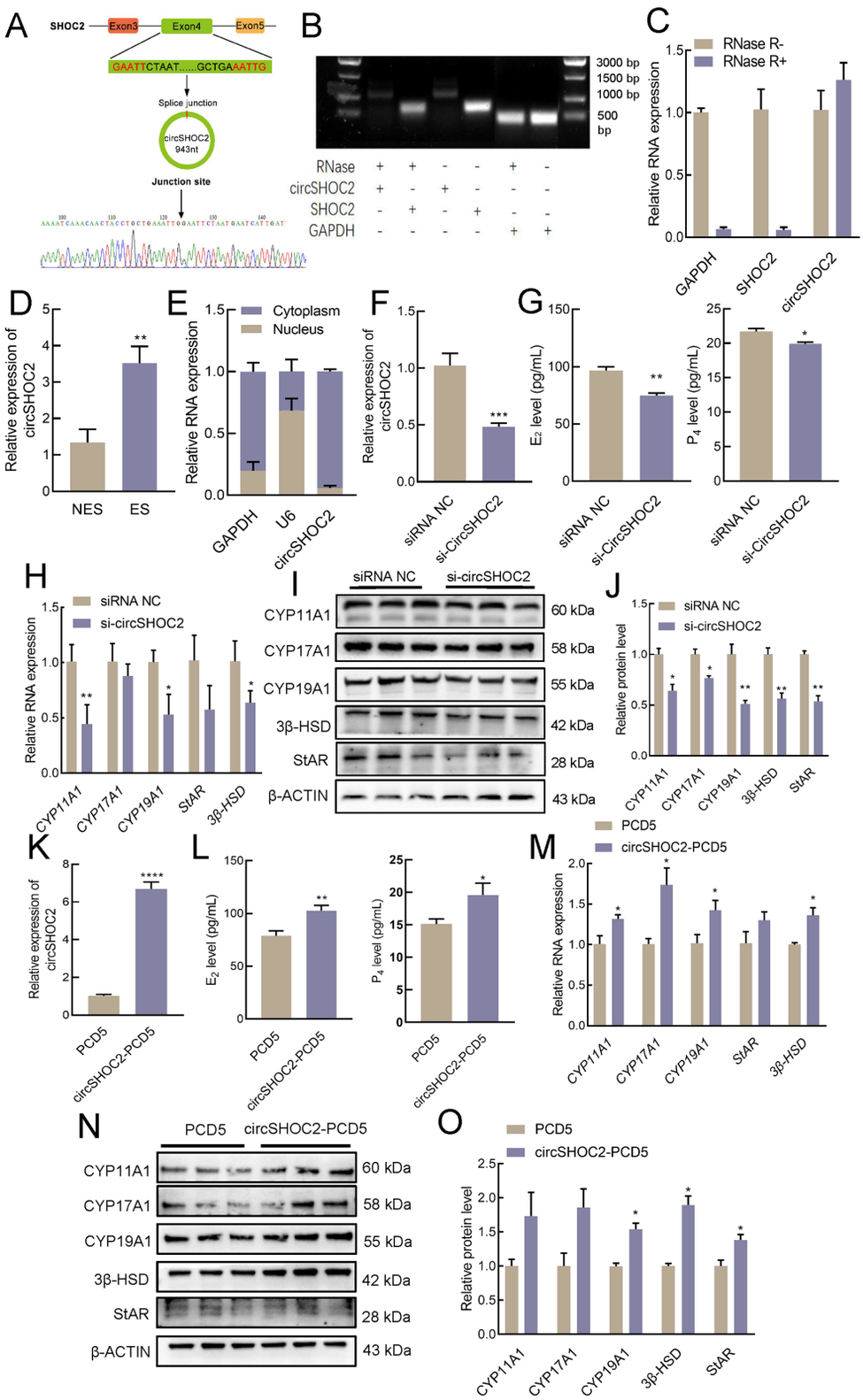

Figure 3 Effect of circSHOC2 on steroid hormone synthesis in ovarian GCs

A: Schematic representation of circSHOC2 structure. B: Detection of circSHOC2 and SHOC2 mRNA following RNase R digestion, *n*=3. C: RT-qPCR product electrophoresis following RNase R digestion, *n*=3. D: Validation of circSHOC2 expression in ovarian tissues from ES and NES sows by RT-qPCR, *n*=6. E: RNA detection of circSHOC2 in nuclear and cytoplasmic fractions, *n*=5. F: Efficiency of circSHOC2 knockdown, *n*=5. G: Concentrations of E_2 and P_4 in supernatants based on ELISA, *n*=4. H: mRNA expression levels of genes related to steroid hormone synthesis based on RT-qPCR, *n*=4. I, J: Protein expression levels of steroid hormone synthesis-related genes based on western blot analysis, *n*=3. K: Efficiency of circSHOC2 overexpression, *n*=5. L: Concentrations of E_2 and P_4 in supernatants based on ELISA, *n*=4. M: mRNA expression levels of genes related to steroid hormone synthesis based on RT-qPCR, *n*=4. N, O: Protein expression levels of steroid hormone synthesis-related genes based on western blot analysis, *n*=3. *: $P<0.05$; **: $P<0.01$; ***: $P<0.001$; ****: $P<0.0001$.

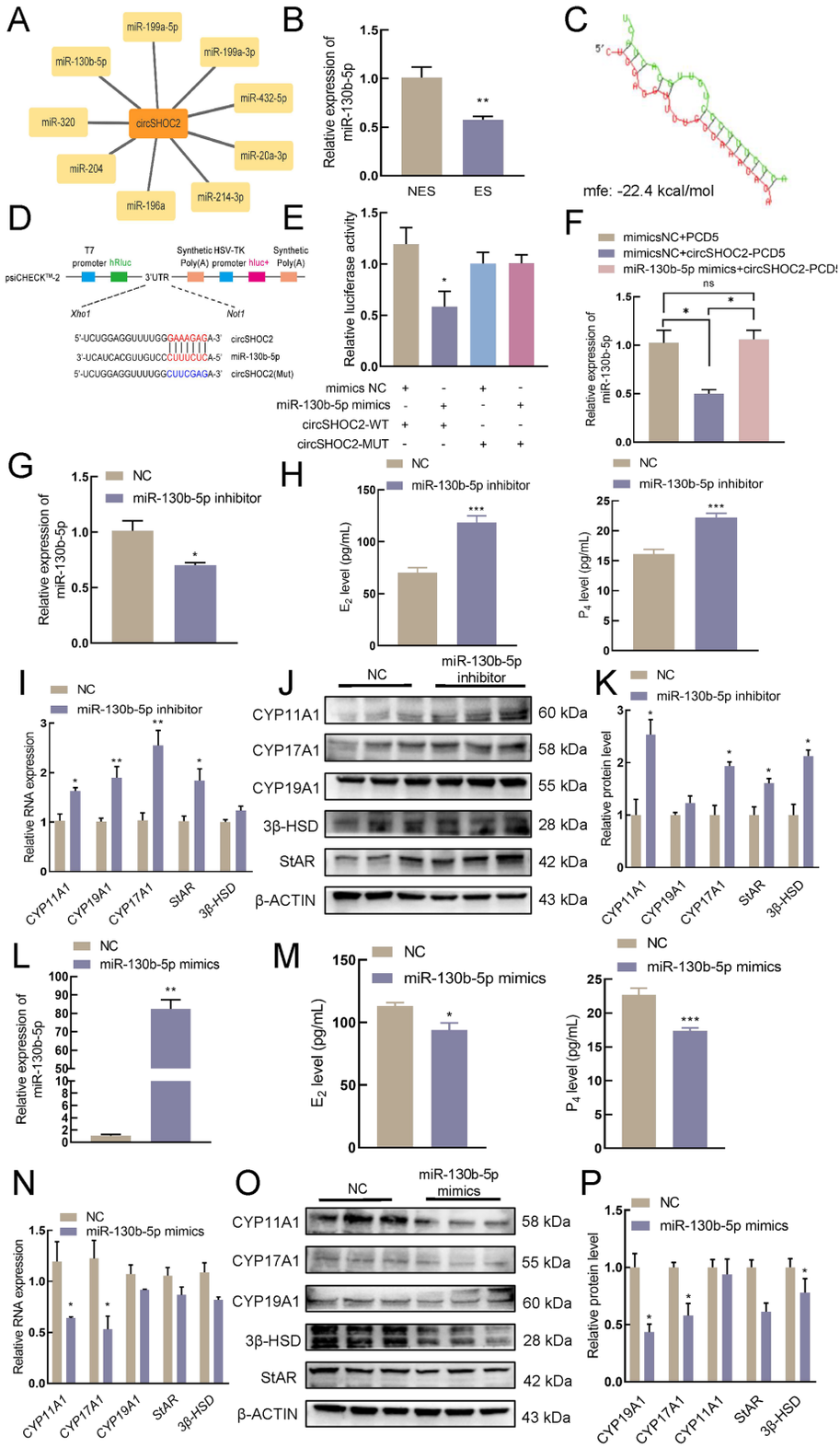

Figure 4 CircSHOC2 sponges miR-130b-5p to regulate steroid hormone synthesis in GCs

A: Predicted miRNA network targeted by circSHOC2. B: RT-qPCR analysis showing miR-130b-5p mRNA expression in ES and NES ovarian tissues, *n*=4. C: Prediction of circSHOC2-miR-130b-5p binding sites. D: Schematic of dual-luciferase reporter vector. E: Results of dual-luciferase reporter assay, *n*=3. F: mRNA expression level of miR-130b-5p following circSHOC2 overexpression and circSHOC2 and miR-130b-5p overexpression, *n*=3. G: Efficiency of miR-130b-5p inhibitor suppression, *n*=4. H: Concentrations of E_2 and P_4 based on ELISA, *n*=6. I: RT-qPCR analysis of steroid hormone synthesis-related gene mRNA expression, *n*=4. J, K: Western blot analysis of steroid hormone synthesis-related protein expression, *n*=3. L: Efficiency of miR-130b-5p mimic overexpression, *n*=4. M: Concentrations of E_2 and P_4 based on ELISA, *n*=6. N: RT-qPCR analysis of steroid hormone synthesis-related gene mRNA expression, *n*=4. O, P: Western blot analysis of steroid hormone synthesis-related protein expression, *n*=3. *: $P<0.05$; **: $P<0.01$; ***: $P<0.001$.

significant reduction in miR-130b-5p expression (Figure 4G), accompanied by marked increases in the concentrations of E_2 and P_4 compared to the control group (Figure 4H). Interference with miR-130b-5p significantly increased the mRNA levels of *CYP17A1*, *CYP19A1*, *CYP11A1*, and *StAR*, as well as the protein levels of CYP11A1, CYP17A1, StAR, and 3β-HSD (Figure 4I, J, L). Conversely, primary GC treatment with miR-130b-5p mimics exerted the opposite effects (Figure 4L), reducing steroid hormone content and the expression of related genes (Figure 4M–P). These findings indicate that miR-130b-5p inhibits the synthesis of E_2 and P_4 in GCs.

Rescue assays revealed that concurrent overexpression of circSHOC2 and miR-130b-5p attenuated circSHOC2-mediated enhancement of steroid hormone production in GCs (Supplementary Figure S3A–C), confirming that circSHOC2 promotes steroidogenesis, at least in part, through sequestration of miR-130b-5p.

CircSHOC2-miR-130b-5p-ASH1L axis modulates steroid hormone synthesis in GCs

Given the conservation of the miR-130b-5p binding site on circSHOC2 across humans, mice, and pigs (Figure 5A), the miRDB, miRWalk, and TargetScan databases were used to predict the target genes of miR-130b-5p. Cross-database analysis yielded 27 candidate genes (Figure 5B). Among these, ASH1L was prioritized based on ovarian expression levels, literature relevance, complete 3'UTR complementarity to the miR-130b-5p seed sequence, favorable binding free energy (−31.0 kcal/mol), and dual-luciferase reporter assay validation (Figure 5C, D). Inhibiting miR-130b-5p increased ASH1L expression, while miR-130b-5p mimics inhibited ASH1L expression (Supplementary Figure S3D, E). Dual-luciferase assays in HEK293T cells confirmed direct regulation of ASH1L by miR-130b-5p. Cotransfection with miR-130b-5p mimics significantly suppressed luciferase activity from one WT ASH1L 3'UTR construct, while no significant change was observed for the other WT construct or mutant version lacking the miR-130b-5p binding site (Figure 5E). These findings demonstrate that ASH1L is a direct target of miR-130b-5p, with regulation dependent on a specific seed-binding site.

To explore the role of ASH1L in steroidogenesis, siRNA-mediated knockdown was performed in porcine GCs (Figure 5F). Compared with the siRNA NC, silencing ASH1L resulted in a significant reduction in E_2 and P_4 secretion (Figure 5G, H). Additionally, the mRNA levels of *CYP11A1*, *CYP17A1*, *CYP19A1*, and *3β-HSD* were significantly reduced, as were the protein levels of CYP17A1 and 3β-HSD (Figure 5I −K). Rescue experiments confirmed that co-transfection of the miR-130b-5p inhibitor with si-ASH1L restored E_2 and P_4 concentrations otherwise suppressed by ASH1L knockdown (Figure 5L–N). Additionally, coexpression of circSHOC2-PCD5 and miR-130b-5p mimics significantly reduced ASH1L expression compared to the control (circSHOC2-PCD5+mimics NC) (Supplementary Figure S3F), indicating that circSHOC2 modulates ASH1L levels through miR-130b-5p sequestration.

DISCUSSION

Comprehensive profiling of porcine ovarian circRNAs has previously revealed expression differences across estrous stages (Niu et al., 2022), between animals with divergent reproductive capacities (Liang et al., 2020), and during physiological processes such as ovarian aging (Xi et al., 2019) and follicular atresia (Guo et al., 2020). However, circRNA landscapes in ES and NES gilts remain unexplored.

In the present study, 5 275 host genes were identified from ovarian circRNAs in ES and NES gilts. Pathway enrichment analysis revealed significant association with TGF signaling, ECM-receptor interaction, actin regulation, and p53 signaling pathways. These pathways are functionally integral to GC physiology. Notably, TGF signaling regulates GC proliferation, apoptosis, and estrogen biosynthesis (Bai et al., 2017; Lundberg et al., 2022); actin remodeling plays a critical role in regulating steroidogenic output (Chen et al., 2023); and p53 signaling governs apoptotic responses in GCs (Joo et al., 2023). These findings suggest that ovarian circRNAs may influence estrous expression by modulating GC survival and steroid hormone synthesis.

The synthesis of steroid hormones represents a fundamental role of ovarian GCs (Bjersing et al., 1964), and accumulating evidence supports a regulatory role for circRNA in this process. For example, circDDX10 expression, which declines with age in human ovaries, inhibits E_2 synthesis when silenced, concomitant with down-regulation of steroidogenic genes (Cai et al., 2021). Similarly, circRPS19, which exhibits differential expression during chicken follicular development, promotes GC proliferation and steroidogenesis via the miR-218-5p/INHBB axis (Wei et al., 2024). In the present study, circSHOC2 emerged as the most significantly differentially expressed circRNA between ES and NES gilts and was subsequently shown to regulate steroidogenesis in GCs by modulating CYP19A1, StAR, and 3β-HSD expression, thereby enhancing E_2 and P_4 synthesis.

CircRNAs typically regulate cellular processes by functioning as competing endogenous RNAs (ceRNAs) that sequester specific miRNAs. For example, circ0001470 promotes embryonic development by sponging miR-140-3p and modulating PTGFR expression (Zhang et al., 2022a), while circKDM5B enhances porcine blastocyst development by regulating trophoblast barrier function through sponging miR-128 (Gao et al., 2023a). In the current study, miR-130b-5p—abundantly expressed in the ovaries of NES gilts—was identified as a direct target of circSHOC2. Previous studies have shown that miR-130b-5p regulates cell proliferation (Zhang et al., 2019) and lipid metabolism (Feng et al., 2024), and that miR-130a-5p can be sponged by circWHSC1 (Shi et al., 2023a). These findings suggest that miR-130b-5p may similarly regulate the cellular state of GCs, thereby affecting cell function. Here, dual-luciferase assays confirmed the interaction between miR-130b-5p and circSHOC2, and rescue experiments demonstrated that circSHOC2 promotes E_2 and P_4 synthesis in GCs through miR-130b-5p sequestration. These results provide the first evidence that miR-130b-5p directly regulates steroid hormone biosynthesis in porcine GCs.

ASH1L was identified as a downstream target of miR-130b-5p through integrative miRNA target prediction. ASH1L functions as a key epigenetic regulator (Xi et al., 2020), with evidence from bovine cumulus cells indicating that its knockdown can significantly suppress cell proliferation, promote apoptosis, and reduce H3K36me1/2/3 methylation (Cui et al., 2021). Although the direct involvement of H3K36 methylation in regulating steroidogenic enzymes remains unclear, ASH1L is known to colocalize with H3K4me3 and modulate histone methylation dynamics (Vann et al., 2025). Furthermore, epigenetic studies have identified functional H3K4me3 regulatory elements in the promoter regions of key steroidogenic genes, including CYP19A1 (Madogwe et al.,

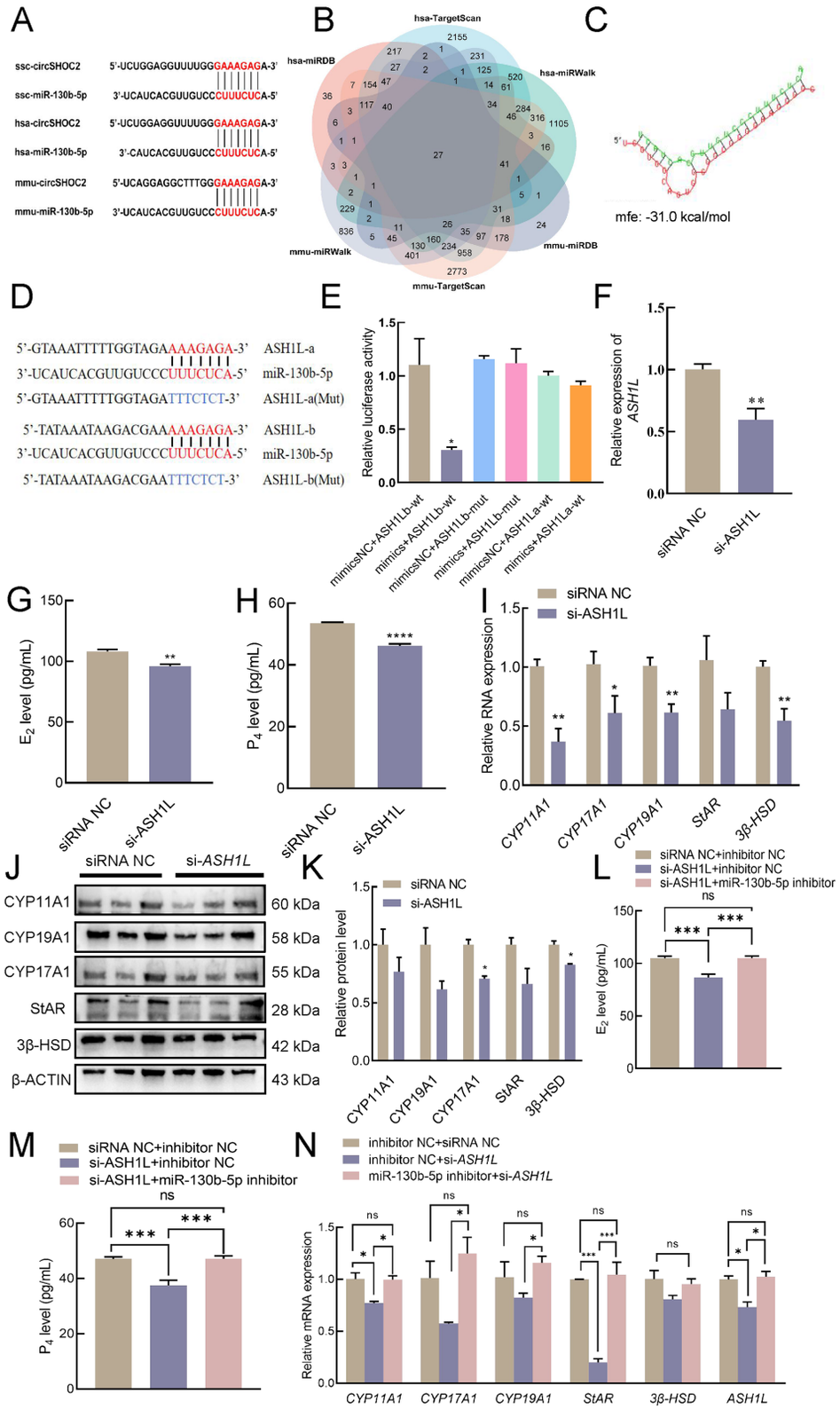

Figure 5 MiR-130b-5p targets and inhibits ASH1L to regulate steroid hormone synthesis in GCs

A: Binding sites of circSHOC2 and miR-130b-5p in humans, mice, and pigs. B: Screening for target genes via multiple databases. C: Prediction of binding sites. D: Schematic of two ASH1L dual-luciferase reporter vectors. E: Dual-luciferase activity assay. F: Inhibition efficiency of si-ASH1L, *n*=3. G: Concentration of E_2 based on ELISA, *n*=4. H: Concentration of P_4 based on ELISA, *n*=4. I: mRNA expression levels of steroid hormone synthesis-related genes based on RT-PCR, *n*=4. J, K: Protein expression levels of steroid hormone synthesis-related genes based on western ^{blot} analysis, *n*=3. L: Concentration of E_2 based on ELISA, *n*=5. M: Concentration of P_4 based on ELISA, *n*=5. N: mRNA expression levels of steroid hormone synthesis-related genes, *n*=3. ns: Not significant; *: P<0.05; **: P<0.01; ***: P<0.001; ****: P<0.0001. ssc: *Sus scrofa*; hsa: *Homo sapiens*; mmu: *Mus musculus*.

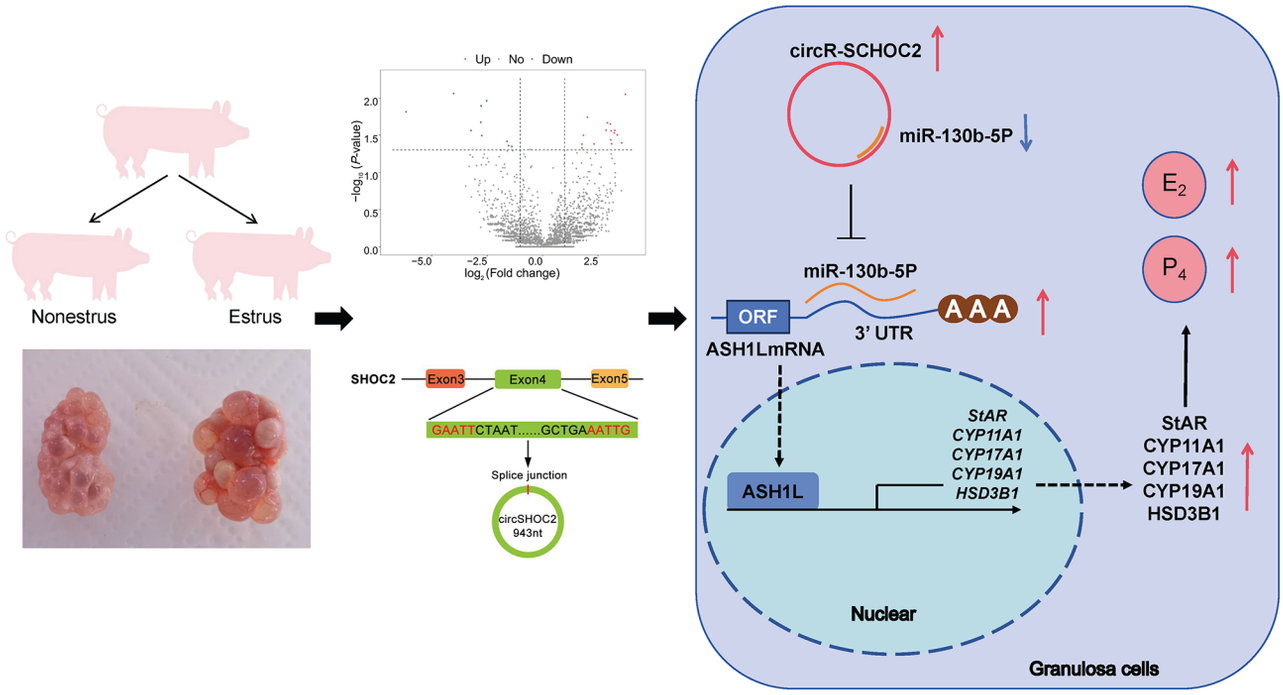

Figure 6 Schematic model illustrating how circSHOC2, identified through circRNA sequencing of ES and NES ovaries, regulates E_2 and P_4 synthesis in ovarian granulosa cells (GCs) via the miR-130b-5p/ASH1L axis

2020), CYP11A1 (Okada et al., 2016), and StAR (Li et al., 2024). These findings suggest that ASH1L may regulate steroidogenesis by modulating H3K4me3 modifications. However, the mechanistic link between ASH1L-mediated histone modification and transcriptional regulation of steroidogenic pathways remains unresolved and will be the focus of future investigations.

While estrus regulation involves a complex molecular network, this study specifically examined the function of circSHOC2 in GCs. Ongoing work will aim to characterize additional circRNAs, expand the ceRNA interaction landscape, and refine the regulatory architecture governing steroid hormone biosynthesis in porcine ovaries

In summary, this study identified circSHOC2 as a key regulatory circRNA that regulates the synthesis of E_2 and P_4 in ovarian GCs via the circSHOC2/miR-130b-5p/ASH1L axis, offering novel insights into the molecular regulation of reproductive function in replacement gilts.

CONCLUSION

CircRNA sequencing of ovarian tissues from ES and NES gilts identified circSHOC2 as a differentially expressed circRNA that regulates the synthesis of E_2 and P_4 in ovarian GCs via the circSHOC2/miR-130b-5p/ASH1L axis (Figure 6).

DATA AVAILABILITY

The datasets used and analyzed in the current study are available from the corresponding author upon reasonable request. The raw RNA-seq data analyzed in this study are available from the China National Center for Bioinformation database of the Genome Sequence Archive (GSA) (CRA023794), National Center for Biotechnology Information (NCBI) (GSE295579, PRJNA1255211), and Science Data Bank (DOI: 10.57760/sciencedb.22113).

SUPPLEMENTARY DATA

Supplementary data to this article can be found online.

COMPETING INTERESTS

The authors declare that they have no competing interests.

AUTHORS' CONTRIBUTIONS

L.T.Z., T.Z., and X.R.S. performed the experiments and composed the first draft. M.M.L. and Y.H.L. performed the experiments. L.G. and G.S.Y. guided the experiments. G.Y.C. polished and finalized the article and conceived and directed the project. All authors read and approved the final version of the manuscript.

ACKNOWLEDGMENTS

The authors gratefully acknowledge all the teachers and students from the Laboratory of Animal Fat Deposition & Muscle Development. Thanks to Prof. Shi-Min Liu from the University of Western Australia for revising the language of the manuscript.

REFERENCES

Am-In N, Suwimonteerabutr J, Kirkwood RN. 2020. Serum anti-mullerian hormone and estradiol concentrations in gilts and their age at puberty. *Animals*, **10**(11): 2189.

Anders S, Pyl PT, Huber W. 2015. HTSeq—a Python framework to work with high-throughput sequencing data. *Bioinformatics*, **31**(2): 166–169.

Bai L, Chu GY, Wang WS, et al. 2017. BAMBI promotes porcine granulosa cell steroidogenesis involving TGF-β signaling. *Theriogenology*, **100**: 24–31.

Bjersing L, Cartensen H. 1964. The role of the granulosa cell in the biosynthesis of ovarian steroid hormones. *Biochimica et Biophysica Acta (BBA) - General Subjects*, **86**(3): 639–640.

Brinkmeier ML, Geister KA, Jones M, et al. 2015. The histone methyltransferase gene absent, small, or homeotic discs-1 like is required for normal hox gene expression and fertility in mice. *Biology of Reproduction*, **93**(5): 121.

Cai HC, Chang TL, Li YM, et al. 2021. Circular *DDX10* is associated with ovarian function and assisted reproductive technology outcomes through modulating the proliferation and steroidogenesis of granulosa cells. *Aging*, **13**(7): 9592–9612.

Chen D, Wu CQ, Wei SM, et al. 2023. Semaphorin 4C regulates ovarian

steroidogenesis through RHOA/ROCK1-mediated actin cytoskeleton rearrangement. *Molecular Human Reproduction*, **29**(5): gaad010.

Chen H, Yang YQ, Wang J, et al. 2018. miR-130b-5p promotes proliferation, migration and invasion of gastric cancer cells via targeting RASAL1. *Oncology Letters*, **15**(5): 6361–6367.

Cui LX, Tian YQ, Hao HS, et al. 2021. Knockdown of ASH1L methyltransferase induced apoptosis inhibiting proliferation and H3K36 methylation in bovine cumulus cells. *Theriogenology*, **161**: 65–73.

Dial GD, Dial OK, Bevier GW, et al. 1983. Estrous behavior and circadian discharge of luteinizing hormone in the prepubertal gilt in response to exogenous estrogen. *Biology of Reproduction*, **29**(5): 1047–1056.

Domingues RR, Wiltbank MC, Hernandez LL. 2023. The antidepressant fluoxetine (Prozac®) modulates estrogen signaling in the uterus and alters estrous cycles in mice. *Molecular and Cellular Endocrinology*, **559**: 111783.

Feng K, Wu YK, Li JG, et al. 2024. Critical role of mir-130b-5p in cardiomyocyte proliferation and cardiac repair in mice after myocardial infarction. *Stem Cells*, **42**(1): 29–41.

Feng T, DeVore AA, Perego MC, et al. 2019. Effects of N-carbamylglutamate and arginine on steroidogenesis and proliferation of pig granulosa cells *in vitro*. *Animal Reproduction Science*, **209**: 106138.

Fu Y, Jiang H, Liu JB, et al. 2018. Genome-wide analysis of circular RNAs in bovine cumulus cells treated with BMP15 and GDF9. *Scientific Reports*, **8**(1): 7944.

Gao D, Wang X, Yan YL, et al. 2023a. *CircKDM5B* sponges *miR-128* to regulate porcine blastocyst development by modulating trophectoderm barrier function. *Molecular Human Reproduction*, **29**(9): gaad027.

Gao L, Zhang LT, Zhang YL, et al. 2023b. miR-10a-5p inhibits steroid hormone synthesis in porcine granulosa cells by targeting CREB1 and inhibiting cholesterol metabolism. *Theriogenology*, **212**: 19–29.

Gao Y, Wang JF, Zhao FQ. 2015. CIRI: an efficient and unbiased algorithm for *de novo* circular RNA identification. *Genome Biology*, **16**(1): 4.

Geisert RD, Bazer FW, Lucas CG, et al. 2024. Maternal recognition of pregnancy in the pig: A servomechanism involving sex steroids, cytokines and prostaglandins. *Animal Reproduction Science*, **264**: 107452.

Guo TY, Huang L, Yao W, et al. 2020. The potential biological functions of circular RNAs during the initiation of atresia in pig follicles. *Domestic Animal Endocrinology*, **72**: 106401.

Jeck WR, Sorrentino JA, Wang K, et al. 2013. Circular RNAs are abundant, conserved, and associated with ALU repeats. *RNA*, **19**(2): 141–157.

Jia WC, Xu B, Wu J. 2018. Circular RNA expression profiles of mouse ovaries during postnatal development and the function of circular RNA epidermal growth factor receptor in granulosa cells. *Metabolism*, **85**: 192–204.

Joo NR, Park SA, Park JH, et al. 2023. TOPK inhibits TNF-α-induced granulosa cell apoptosis via regulation of SIRT1/p53. *Biochemical and Biophysical Research Communications*, **664**: 128–135.

Kim D, Langmead B, Salzberg SL. 2015. HISAT: a fast spliced aligner with low memory requirements. *Nature Methods*, **12**(4): 357–360.

Knox RV. 2024. Swine fertility in a changing climate. *Animal Reproduction Science*, **269**: 107537.

Kolesarova A, Medvedova M, Halenar M, et al. 2017. The influence of deoxynivalenol and zearalenone on steroid hormone production by porcine ovarian granulosa cells *in vitro*. *Journal of Environmental Science and Health, Part B*, **52**(11): 823–832.

Langendijk P, van den Brand H, Soede NM, et al. 2000. Effect of boar contact on follicular development and on estrus expression after weaning in primiparous sows. *Theriogenology*, **54**(8): 1295–1303.

Li FP, Yang R, Lu L, et al. 2024. Comparative steroidogenic effects of hexafluoropropylene oxide trimer acid (HFPO-TA) and perfluorooctanoic acid (PFOA): Regulation of histone modifications. *Environmental Pollution*, **350**: 124030.

Li G, Ye ZS, Shi C, et al. 2017. The histone methyltransferase ash1l is required for epidermal homeostasis in mice. *Scientific Reports*, **7**: 45401.

Liang GM, Yan JY, Guo J, et al. 2020. Identification of ovarian circular RNAs and differential expression analysis between MeiShan and large white pigs. *Animals (Basel)*, **10**(7): 1114.

Liang GM, Yang YL, Niu GL, et al. 2017. Genome-wide profiling of *Sus scrofa* circular RNAs across nine organs and three developmental stages. *DNA Research*, **24**(5): 523–535.

Liu MZ, Zhang CL, Chen JH, et al. 2024. Characterization and analysis of transcriptomes of multiple tissues from estrus and diestrus in pigs. *International Journal of Biological Macromolecules*, **256**: 128324.

Liu XN, Chen SH, Zhang LJ. 2020. Downregulated microRNA-130b-5p prevents lipid accumulation and insulin resistance in a murine model of nonalcoholic fatty liver disease. *American Journal of Physiology-Endocrinology and Metabolism*, **319**(1): E34–E42.

Lundberg AL, Jaskiewicz NM, Maucieri AM, et al. 2022. Stimulatory effects of TGFα in granulosa cells of bovine small antral follicles. *Journal of Animal Science*, **100**(7): skac105.

Ma BC, Wang SH, Wu WZ, et al. 2023. Mechanisms of circRNA/lncRNA-miRNA interactions and applications in disease and drug research. *Biomedicine & Pharmacotherapy*, **162**: 114672.

Madogwe E, Tanwar DK, Taibi M, et al. 2020. Global analysis of FSH-regulated gene expression and histone modification in mouse granulosa cells. *Molecular Reproduction and Development*, **87**(10): 1082–1096.

McGlone JJ, Duke L, Sanchez M, et al. 2023. Self-administration of a boar priming pheromone stimulates puberty in gilts without boar exposure. *Animals (Basel)*, **14**(1): 91.

Miyazaki H, Higashimoto K, Yada Y, et al. 2013. Ash1l methylates Lys36 of histone H3 independently of transcriptional elongation to counteract polycomb silencing. *PLoS Genetics*, **9**(11): e1003897.

Niu X, Huang YL, Lu H, et al. 2022. CircRNAs in Xiang pig ovaries among diestrus and estrus stages. *Porcine Health Management*, **8**(1): 29.

Okada M, Lee L, Maekawa R, et al. 2016. Epigenetic changes of the cyp11a1 promoter region in granulosa cells undergoing luteinization during ovulation in female rats. *Endocrinology*, **157**(9): 3344–3354.

Patop IL, Wüst S, Kadener S. 2019. Past, present, and future of circRNAs. *The EMBO Journal*, **38**(16): e100836.

Rodway MR, Swan CL, Crellin NK, et al. 1999. Steroid regulation of progesterone synthesis in a stable porcine granulosa cell line: a role for progestins. *The Journal of Steroid Biochemistry and Molecular Biology*, **68**(5-6): 173–180.

Shi L, Zhao YS, Liu X, et al. 2023a. Circular RNA circWHSC1 facilitates colorectal cancer cell proliferation by targeting miR-130a-5p/zeb1 signaling *in vitro* and *in vivo*. *Heliyon*, **9**(10): e20176.

Shi SJ, Chu GY, Zhang LT, et al. 2023b. Deubiquitinase UCHL1 regulates estradiol synthesis by stabilizing voltage-dependent anion channel 2. *Journal of Biological Chemistry*, **299**(11): 105316.

Sirotkin AV. 1994. Direct influence of melatonin on steroid, Nona peptide hormones, and cyclic nucleotide secretion by granulosa cells isolated from porcine ovaries. *Journal of Pineal Research*, **17**(3): 112–117.

Ting AY, Xu J, Stouffer RL. 2015. Differential effects of estrogen and progesterone on development of primate secondary follicles in a steroid-depleted milieu *in vitro*. *Human Reproduction*, **30**(8): 1907–1917.

Vann KR, Sharma R, Hsu CC, et al. 2025. Structure-function relationship of ASH1L and histone H3K36 and H3K4 methylation. *Nature Communications*, **16**(1): 2235.

Wei YH, Shen XX, Zhao XY, et al. 2024. Circular RNA circRPS19 promotes chicken granulosa cell proliferation and steroid hormone synthesis by interrupting the miR-218-5p/INHBB axis. *Theriogenology*, **219**: 103–115.

Xi H, Peng Y, Xie WQ, et al. 2020. A chromosome 1q22 microdeletion including *ASH1L* is associated with intellectual disability in a Chinese family.

Molecular Cytogenetics, **13**: 20.

Xi XY, Zou Q, Wei YY, et al. 2019. Dynamic changes of DNA methylation and transcriptome expression in porcine ovaries during aging. *BioMed Research International*, **2019**: 8732023.

Xia M, Liu J, Liu SX, et al. 2017. Ash1l and lnc-Smad3 coordinate *Smad3* locus accessibility to modulate iTreg polarization and T cell autoimmunity. *Nature Communications*, **8**: 15818.

Xin WS, Zhang F, Yan GR, et al. 2018. A whole genome sequence association study for puberty in a large Duroc × Erhualian F2 population. *Animal Genetics*, **49**(1): 29–35.

Xiong WY, Nie JW, Luo JX, et al. 2024. Effects of dietary iron supplementation on reproductive performance of sows and growth performance of piglets. *Journal of Animal Science*, **102**: skae096.

Xu L, Liu C, Na R, et al. 2021. Genetic basis of follicle development in Dazu black goat by whole-transcriptome sequencing. *Animals*, **11**(12): 3536.

Yang SB, Zhou XL, Pei Y, et al. 2018. Identification of differentially expressed genes in porcine ovaries at proestrus and estrus stages using RNA-Seq technique. *BioMed Research International*, **2018**: 9150723.

Zhang L, Zhou CF, Jiang XY, et al. 2022a. Circ0001470 acts as a mir-140-3p sponge to facilitate the progression of embryonic development through regulating PTGFR expression. *Cells*, **11**(11): 1746.

Zhang N N, Hu Z N, Qiang Y, et al. 2019. Circulating miR-130b- and miR-21-based diagnostic markers and therapeutic targets for hepatocellular carcinoma. *Molecular Genetics & Genomic Medicine*, **7**(12): e1012.

Zhang T, Ren TH, Lin H, et al. 2022b. ASH1L contributes to oocyte apoptosis by regulating DNA damage. *American Journal of Physiology-Cell Physiology*, **323**(4): C1264–C1273.

Zhang XO, Dong R, Zhang Y, et al. 2016y. Diverse alternative back-splicing and alternative splicing landscape of circular RNAs. *Genome Research*, **26**(9): 1277–1287.

Ziecik AJ, Drzewiecka K, Gromadzka-Hliwa K, et al. 2020. Altrenogest affects the development and endocrine milieu of ovarian follicles in prepubertal and mature gilts. *Biology of Reproduction*, **103**(5): 1069–1084.